First-principles study of the electronic and optical properties in rhombohedral $LaAlO_3$

Xin Luo and Biao Wang

Citation: Journal of Applied Physics **104**, 053503 (2008); doi: 10.1063/1.2973671

JOURNAL OF APPLIED PHYSICS **104**, 053503 (2008)

First-principles study of the electronic and optical properties in rhombohedral $LaAlO_3$

Xin Luo and Biao Wang[a)]
State Key Laboratory of Optoelectronic Materials and Technologies/Institute of Optoelectronic and Functional Composite Materials, School of Physics and Engineering, Sun Yat-sen University, 510275 Guangzhou, China

(Received 17 April 2008; accepted 25 June 2008; published online 4 September 2008)

In this paper, the electronic structure, chemical bonding, and optical properties of rhombohedral $LaAlO_3$ are investigated by using the full potential linearized augmented plane wave method with the generalized gradient approximation. The analysis of the electronic density profile, Mulliken charge, and bond population shows a combination of the covalent and ionic natures in the chemical bonding. The calculated complex dielectric function is consistent with the experimental data from the ultraviolet spectroscopic ellipsometry measurement. The optical spectra are assigned to the interband transition from O valence to La conduction bands in the low energy region. Furthermore, absorption spectrum, electron energy-loss spectrum, optical conductivity, reflectivity, and refractive index are derived from the complex dielectric function, and the absorption spectrum exhibits an optical band gap of 6.1 eV, which is consistent with several other experimental measurements. © *2008 American Institute of Physics*. [DOI: 10.1063/1.2973671]

I. INTRODUCTION

Nowadays, one of the major challenges in the semiconductor industry is to find a suitable high dielectric constant (high K) gate oxide to replace SiO_2 in microelectronic devices.[1] With the aggressive downscaling of the complementary metal-oxide semiconductor device manufacturing process, the conventional silicon dioxide gate dielectric thickness is approaching its physical limit due to its large leakage current. Since the high K gate oxide has a larger dielectric constant, replacing the SiO_2 gate oxide with a high K material would allow the gate oxide to increase its capacitance without having to reduce its thickness. In addition, the high K gate oxide should have large interface band offsets to Si, high dielectric breakdown strength, few defects in the films, stable interface with Si, and relatively low cost in the fabrication process.[2]

Presently, the leading alternative gate oxides are the HfO_2 and ZrO_2, which are amorphous oxides. However, the semiconductor industry requires an epitaxial dielectric with a sharp interface on Si for the next generation high K materials.[3] Most of the ABO_3 perovskite materials have a large dielectric constant, and $LaAlO_3$ is listed as a candidate for epitaxial gate oxide in the latest International Technology Roadmap for Semiconductors.[3] Crystalline $LaAlO_3$ is a promising candidate for SiO_2 replacement because it has many outstanding features: high dielectric constant (23–25),[4–6] wide energy band gap (5.5–6.5),[7–9] large conduction band offsets with silicon,[8,9] and stable thermal property during the metal-oxide-semiconductor field-effect transistor annealing process.[5] Moreover, there is less than 1% lattice mismatch between the $LaAlO_3$ (001) and Si (001) planes, and the $LaAlO_3$ film can grow epitaxially on the Si substrate. Recently, epitaxial Si films have been grown on $LaAlO_3$ substrate with an atomically well defined interface due to improvements in growth techniques.[10]

There are many first-principles studies focusing on the interface structure,[11] either on the $Si/LaAlO_3$ interface[12] or on the metal gate/$LaAlO_3$ interface,[13] the band offsets,[14] the defect states[15] and surface relaxations,[16] the doping effects on the dielectric properties,[17] and the lattice vibrational modes[18] of crystalline $LaAlO_3$ in both the cubic and rhombohedral phases. Among the recent experimental studies, we mention the x-ray photoelectron spectroscopy (XPS) measurements by Mi *et al.*[9] and the ultraviolet photoelectron spectroscopy reports by Lim *et al.*[7] However, in contrast to the extensive optical experimental measurements,[7,19,20] there is no corresponding theoretical report concerning the optical properties of $LaAlO_3$, which will make a significant contribution in understanding the properties of this material and provide a theoretical framework to discuss the experimental findings mentioned above, suggesting pathways for future research.

In this paper, we present a series of first-principles calculations on the electronic and optical properties of rhombohedral $LaAlO_3$. The optical properties, such as the absorption spectrum and the dielectric function, can be used to determine the optical band gap and electronic dielectric constants, which are fundamental in the modeling of the conduction band offsets, leakage current, and dielectric breakdown.

II. COMPUTATIONAL DETAILS

The calculations were performed in the framework of the density functional theory with the full-potential linearized augmented plane wave (FP-LAPW) method implemented in the latest WIEN2k code.[21] The exchange and correlation effects were treated using the generalized gradient approximation.[22] The lanthanum $6s$, $5d$, $5p$, $5s$, and $4f$ elec-

---

[a)] Author to whom correspondence should be addressed. Electronic mail: wangbiao@mail.sysu.edu.cn.

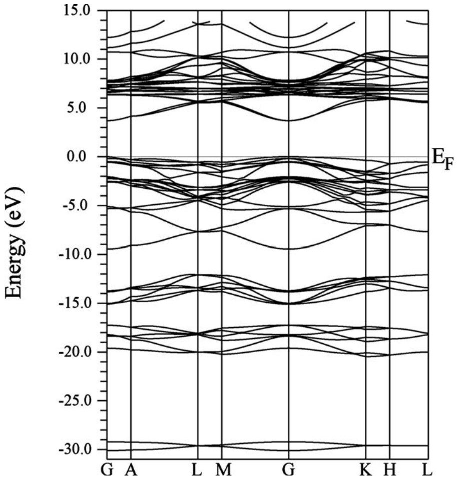

FIG. 1. The energy band structure of rhombohedral $LaAlO_3$ along high symmetry directions in the IBZ.

trons, the aluminum 3*s* and 3*p* electrons, and the oxygen 2*s* and 2*p* electrons were treated as in the valence states. Relativistic effects were taken into account within the scalar-relativistic approximation in the calculation of the valence states and core levels. The muffin-tin sphere radii R_{MT} for La, Al, and O were chosen to be 2.38, 1.68, and 1.68 a.u, respectively. We used the parameter $R_{MT}K_{max}=7.0$ to control the size of the basic set of the wave functions and made the expansion up to $l=12$ in the muffin tins. A $15\times 15\times 15$ mesh was sampled in the irreducible Brillouin zone (IBZ) according to the Monkhorst–Pack method for the optical calculation. Convergence tests indicated that only a few minor changes occur by switching to a denser mesh or to a larger value of $R_{MT}K_{max}$. The self-consistent calculations would be considered to converge only when the integrated energy difference between the two iterations was within 10^{-5} Ry per formula unit.

III. ELECTRONIC STRUCTURE

At room temperature, bulk $LaAlO_3$ has the rhombohedral-central hexagonal structure with space group *R*-3*C*, and it undergoes a phase transition to the simple cubic structure at about 813 K.[23] In both phases, the Al atoms occupy the AlO_6 octahedral sites in the body center while the La atoms are 12-fold coordinated by O atoms. The rhombohedral phase can be formed by the rotation of the AlO_6 polyhedron through a small angle around one of the triaxes in the cubic structure. Since most of the optical experiments were carried out at room temperature, we adopted the rhombohedral hexagonal structure in the calculation. After the total energy minimization and full lattice and atomic relaxation were conducted, the lattice parameters of the rhombohedral $LaAlO_3$ are found to be $a=b=5.370$ Å and $c=13.138$ Å, which are in agreement with the neutron powder diffraction experiment:[24] $a=b=5.365$ Å and $c=13.111$ Å.

The band structure of $LaAlO_3$ along the high symmetry directions is shown in Fig. 1, while in Fig. 2 we show the total, site, and angular momentum decomposed densities of states (DOSs) of $LaAlO_3$. From these figures, we can see that the top of the valence bands between 0 and −9.4 eV are mostly composed of O 2*p* states with some mixture of Al *sp* and La *p* states. Our site decomposed DOS also shows that the DOS at the Fermi level is dominated by O 2*p* states. Even though considerable amount of Al *p* and La *p* states are present in the occupied part of the DOS, their contribution at the Fermi level is very small. Below the O 2*p* bands are the La 5*p* states that occupy the energy range of −12.0 and −15.1 eV. The energy bands between −17.2 and −20.2 eV mainly consist of O 2*s* states with some admixture of the La *sp* derived states. The bottom of the conduction band is composed of La 5*d* states. There is a direct band gap of 3.95 eV at the gamma point of the band structure. The direct band gap is smaller than the optical band gap that will be discussed later in more detail. The La 5*d* states extend from 3.95 to 10.0 eV and separated by some condense La 4*f* conduction bands in the regions of 6.2 and 7.2 eV. The DOS curves show that the major part of the strong peak in the conduction band is due to the contribution of the La 4*f* states, corresponding to the localized La 4*f* states observed in the band structure. The overall topology of our DOS curves is found to be in agreement with the x-ray photoemission spectrum.[25] The band structure calculated here is consistent with the universal electronic structure for the transition metal/rare earth oxide[26] in which the highest occupied valence bands are derived from O 2*p* states, while the lowest conduction bands are derived from the transition metal *d* states. These *d* states appear as doublets in the unoccupied bands and separate the optical band gap with the ionic gap.

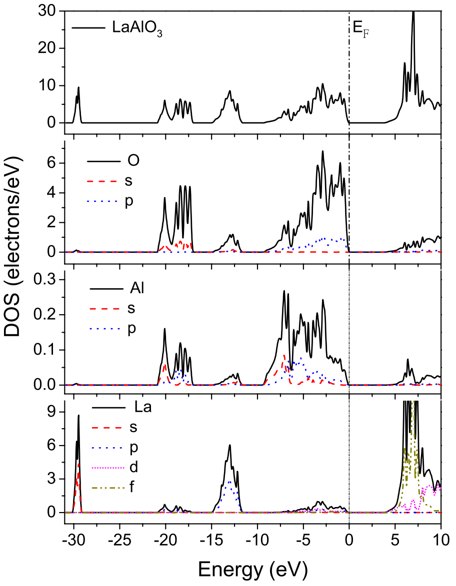

FIG. 2. (Color online) Angular momentum and site decomposed electron DOS of rhombohedral $LaAlO_3$.

In order to investigate the bonding character of the system, we calculated the electronic density distribution as shown in Fig. 3. The contour map was projected along the ⟨110⟩ direction, and there was a dense mixture of charge density between the La–O and Al–O atoms. The interesting aspect of this figure is the presence of a strong directional bonding between the Al atoms and O atoms. There is a weaker covalent bonding between La–O atoms for their rela-

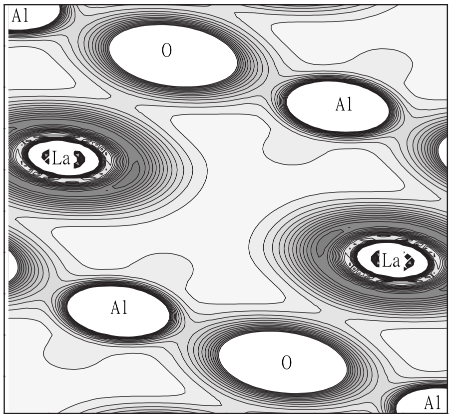

FIG. 3. The electronic density profiles for rhombohedral $LaAlO_3$ in the (110) plane.

tively sparse hybridizations. This directionality between bonding may contribute to the anisotropy in elastic properties and cause the brittleness of $LaAlO_3$. Our angular momentum and site decomposed DOS given in Fig. 2 show that the O *sp* states are strongly mixed with the Al *sp* states over the whole range of the valence band, indicating large Al–O hybridization. This observation is important for the bonding in $LaAlO_3$ and is in agreement with the conclusion from the other ABO_3 perovskite studies. To investigate the chemical bonding behavior in-depth, we also performed the corresponding Mulliken charge and bond population for the $LaAlO_3$ to analyze the bonding character quantitatively. The results are given in Table I. The overlap population between the O–Al atoms is 0.39 e, which is larger than the O–La value of 0.18 e, and both bonding show the covalent nature. The length of O–Al bonding is shorter than that of the O–La bonding. The Mulliken charges transferred from La atoms and Al atoms to O atoms are 1.44 and 1.31 e, respectively. The transferred Mulliken charges indicate that O atoms are more attractive to the itinerant electrons in the O–La bonding than those in the O–Al bonding. From the charge transfer, we can also infer that the Al atoms are more electron affinitive than La atoms. The difference between the formal ionic charge and the Mulliken charge indicates the levels of the ionic bond, and a value of zero indicates a perfectly ionic bond. Because the calculated transferred charge indicates some ionic interaction between the elements, it is obvious that the bonding behavior of $LaAlO_3$ is a combination of ionic and covalent natures.

IV. OPTICAL PROPERTIES

TABLE I. Mulliken charge (*e*) and bond population of rhombohedral $LaAlO_3$.

Species	*s*	*p*	*d*	Total	Charge	Bonds	Population	Length (Å)
La	2.29	6.06	1.22	9.56	1.44	O–La	0.18	2.61
Al	0.58	1.11	0.00	1.69	1.31	O–Al	0.39	1.90
O	1.84	5.08	0	6.92	−0.92	O–O	−0.12	2.68

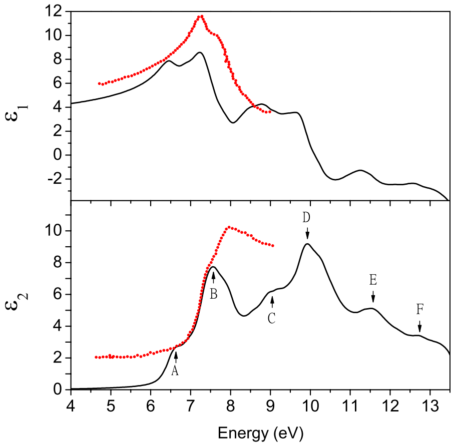

FIG. 4. (Color online) The real $\varepsilon_1(\omega)$ and imaginary $\varepsilon_2(\omega)$ parts of the $LaAlO_3$ dielectric function $\varepsilon(\omega)$. The curves are plotted using a Lorentzian broadening of 0.1 eV. The experimental data of Ref. 7 are depicted by closed dots.

The optical properties of $LaAlO_3$ is determined by the dielectric function $\varepsilon(\omega)=\varepsilon_1(\omega)+i\varepsilon_2(\omega)$ that is mainly contributed from the electronic structures. The imaginary part $\varepsilon_2(\omega)$ of the dielectric function $\varepsilon(\omega)$ is calculated from the momentum matrix elements of transition between the occupied and unoccupied electronic states and is given by

$$\varepsilon_2 = \frac{2e^2\pi}{\Omega\varepsilon_0}\sum_{k,v,c} |\langle\psi_k^c|\hat{u}\, r|\psi_k^v\rangle|^2 \delta(E_k^c - E_k^v - E),$$

where Ω is the unit cell volume, $\hat{u}$ is the vector defining the polarization of the incident electric field, ω is the light frequency, e is the electronic charge, and ψ_k^c and ψ_k^v are the conduction and valence band wave functions at $\mathbf{k}$, respectively. Since the dielectric function describes the causal response, the real and imaginary parts are linked using the Kramers–Kronig transform. The real part $\varepsilon_1(\omega)$ of the dielectric function can be derived from the imaginary part $\varepsilon_2(\omega)$ with the causal transform. In our calculation, the dielectric function is calculated from the momentum matrix between the interband transition directly without a scissors approximation operation. The optical band gap problem is not severe for $LaAlO_3$ due to the small discrepancy between the calculated optical band gap that we will discuss in detail later (about 6.1 eV) and the experimental value (ultraviolet spectroscopic ellipsometry measurement gives 6.3 eV).[20] Figure 4 shows the frequency-dependent complex dielectric function of the rhombohedral $LaAlO_3$. The dotted lines represent the experimental data,[7] while the solid line of the imaginary part $\varepsilon_2(\omega)$ is calculated using the FP-LAPW method. From the real part $\varepsilon_1(\omega)$ of the dielectric function, we can obtain the electronic contribution of the dielectric constants, which is about 4 in our calculation, combining with the lattice vibration contribution of 23 calculated from linear and nonlinear responses method within the density functional perturbation theory (DFPT) embedded in the ABINIT package. The total static dielectric constant is 27. The value is 9% larger than the measured value[27,28] but is consistent with other theoretical prediction.[18] In the imaginary part $\varepsilon_2(\omega)$, the shoulder at 6.5 eV corresponded mainly to the transition from O 2*p* to La 4*f*. Peaks *B* (7.5 eV) and shoulder *C* (9.0 eV) are ascribed to the transition between the O 2*p* and La 5*d*

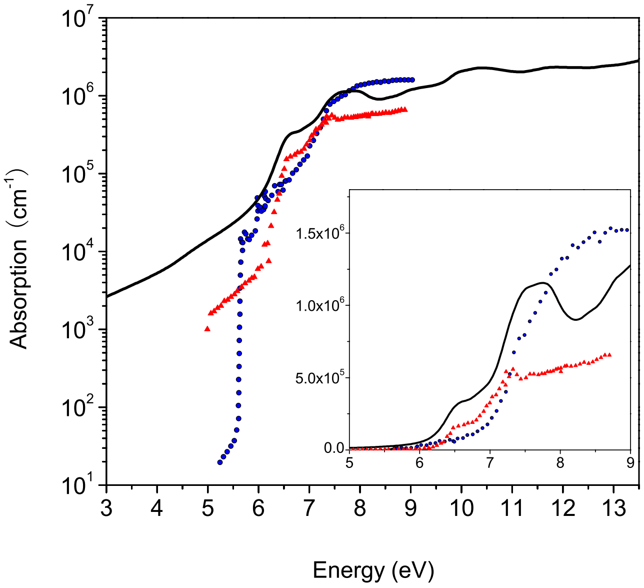

FIG. 5. (Color online) The absorption spectrum of $LaAlO_3$ in the logarithmic coordinates. The calculated curve is shown in solid line, while the experimental data of Refs. 7 and 20 are depicted by short dots and closed triangles, respectively. The inset shows the corresponding results in the linear coordinates at the range of the experimental measurement.

states. The transitions between O 2*p* and La 6*s* are responsible for the other higher energy peaks, such as those at *D* (9.9 eV), *E* (11.5 eV), and *F* (12.7 eV). At low frequency range, there are two steep rises in $\varepsilon_2(\omega)$, one occurs at 6.1 and the other at 7.0 eV. The former value is the optical band gap, while the latter one is the ionic gap. In the $\varepsilon_2(\omega)$ experimental measurement, the optical band gap was not detected.[7] There is a peak at 7.9 eV and the ionic gap is 7.0 eV, derived from the steepest rise in the low energy. Our calculated spectrum for $\varepsilon_2(\omega)$ agrees well with the experimental result.[7]

All the other optical properties, such as the absorption spectrum, the refractive index, the optical conductivity, the energy-loss spectrum, and the reflectivity can be derived from $\varepsilon_1(\omega)$ and $\varepsilon_2(\omega)$. The calculated results of the absorption spectrum and the experimental values are shown in Fig. 5. The absorption coefficient indicates the fraction of energy lost by the electromagnetic wave when it passes through a unit thickness of the material, and it is proportional to the rate of Joule heat produced in the sample. In our calculation, we only consider the eigen absorption, without considering the polarized absorption, which has a minor influence on the spectrum. The steepest increase in the absorption coefficient defines the optical band gap. A value of 6.1 eV is extracted from our calculation, which is in agreement with the previous discussion derived from the threshold rise in $\varepsilon_2(\omega)$. The experimental data of Lim *et al.*[7] and Cicerrella *et al.*[20] are depicted by the short dots and closed triangles, respectively. The corresponding absorption spectrum with linear coordinates in the experimental energy range is shown in the inset, where the absorption threshold can be seen roughly. Our results are slightly larger than the value of 5.6 eV obtained by Lim *et al.*,[7] but is in agreement with the experimental value reported by Cicerrella *et al.*[20] who used the ultraviolet spectroscopic ellipsometry to obtain an optical band gap of 6.3 eV, and also agrees well with the XPS performed by Edge *et al.*[8] and by Mi *et al.*[9] Various experimental values of the band gap between 5.5 and 6.55 eV were reported by different groups. One probable reason is the different microstructures of the sample synthesized on different experimental conditions. Our calculation is based on the ideal atomic structure. Thus the calculated optical band gap provides a useful reference to the study of experiment.

It is interesting to note that the calculated optical band gap from the absorption spectrum does not coincide with the direct band gap as shown in the band structure in Fig. 1. One of the possible reasons for such a discrepancy is the presence of the selection rules between the transition in valence and conduction bands. The transitions between the occupied and unoccupied states are caused by the electric field of the photon. The excitations can be called either plasmons or single particle excitations depending on their collective mode. The spectra resulting from these excitations can be thought of as a joint DOS between the occupied valence bands and the unoccupied conduction bands, weighted by the appropriate matrix elements. Since most of the band gaps of insulator or semiconductor are determined optically, such as the ultraviolet spectroscopic ellipsometry measurement, the electron-energy-loss spectroscopy, and the XPS measurement, if we consider the transition forbidden and selection rules, the optical band gap is usually larger than the direct band gap calculated from the density functional theory. In that sense, the band gap problem induced by the exchange-correlation potential approximation in DFT is not so severe in this calculation. It is important to bear in mind the difference between two band gap concepts while comparing the theoretical results with the corresponding experimental values.

To have more insight into the optical properties in $LaAlO_3$, the calculated results of electron energy-loss spectrum (EELS), optical conductivity, reflectivity, and refractive index are shown in Figs. 6(a)–6(d). In our calculation, we used a Gaussian smearing of 0.3 eV. The energy loss spectrum describes the energy lost by an electron passing through a homogeneous dielectric material.[29] Its main peak is generally defined as the bulk plasma oscillation frequency ω_p, whose position corresponds to ε_1, reaches the zero point, with the condition that $\varepsilon_2 < 1$, and is reasonably smooth.[30] The peak of the EELS calculated using our FP-LAPW method is at about 27.0 eV, corresponding to the inelastic plasmon scattering from outer-shell electrons, whose energy coordinate is accompanied with the sharp reduction in the reflectance. This process is associated with the transitions from the filled O 2*s* bands, lying below the valence band, to the empty La 4*f* conduction bands. There is an additional Raman-scattering peak at 16.4 eV in the EELS due to a net transition of 5*p* electron to the 4*f* orbit, which is in excellent agreement with the experimental energy-loss spectra results of 16.3 eV.[31] The calculated reflectivity has a maximum value of roughly 73% at about 25.8 eV in the range from 0 to 6 eV. The reflectivity is lower than 20%, which indicates that $LaAlO_3$ material is transmitting for photons with energy less than 6 eV. Furthermore, the reflectivity decays gradually as the imaginary part of the refraction *k*, which describes the absorbed energy of the material, approaches zero and the

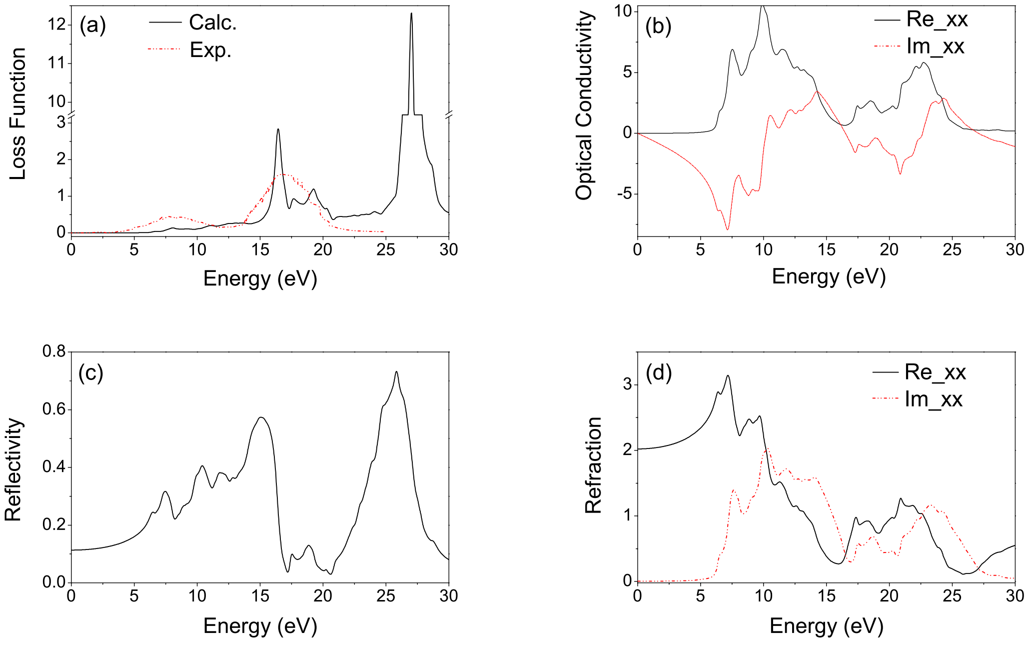

FIG. 6. (Color online) The calculated optical properties of the $LaAlO_3$ as a function of energy: (a) EELS, (b) optical conductivity, (c) reflectivity, and (d) refractive index. The dash-dot lines in EELS denote the corresponding experimental value of Ref. 31

material becomes transparent. From the real part of the refraction, the low frequency static refractive index is equal to 2.0. There are also several peaks in the optical conductivity spectrum that can be assigned to the charge transfer between interbands. Detailed information of the large conductivity spectral weight change at low frequency is especially important for the analysis of the interaction of the localized 4*f* electrons and the delocalized split bands in lanthanum compounds.

V. CONCLUSIONS

In conclusion, we have studied the electronic structure, the chemical bonding, and the optical properties of rhombohedral $LaAlO_3$ using first-principles calculations. The band structure and electron density of the system were obtained, and the bonds exhibited a combination of the covalent and ionic natures. We further present studies of the optical properties of $LaAlO_3$ using the long wavelength approximation. The dielectric function was obtained within linear response theory, with full matrix elements. Our calculated complex dielectric function was shown to agree well with the experimental measurements. From the dielectric function, the other optical properties, such as absorption spectrum, EELS, optical conductivity, reflectivity, and refractive index, can be obtained. We extracted the optical band gap from the calculated absorption spectrum. The value of 6.1 eV is in agreement with recent ultraviolet spectroscopic ellipsometry measurements. It is interesting to note that the discrepancy between the optical band gap and the direct band gap is due to the limitation of the selection rules in the interband transitions. Our investigations provide useful information in the microelectronic design and invite future measurements that will allow a full comparison between theory and experiments.

ACKNOWLEDGMENTS

The authors thank C. L. Li and X. Y. Lu for stimulating discussions. This work was supported by the National Natural Science Foundation of China (NNSFC) (Grant Nos. 10572155 and 10732100) and the Ministry of Education PRC Special Scientific Research Fund for Doctor Subjects in Colleges and Universities (Grant No. 20060558070).

[1] The International Technology Roadmap for Semiconductor, 2007 (http://public.itrs.net).
[2] J. Robertson, Rep. Prog. Phys. **69**, 327 (2006).
[3] B. J. Kennedy and T. Vogt, Mater. Res. Bull. **37**, 77 (2002).
[4] B. E. Park and H. Ishiwara, Appl. Phys. Lett. **82**, 1197 (2003).
[5] W. Xiang, H. Lü, L. Yan, H. Guo, L. Liu, Y. Zhou, G. Yang, J. Jiang, H. Cheng, and Z. Chen, J. Appl. Phys. **93**, 533 (2003).
[6] Y. G. Makeev, A. P. Motornenko, N. T. Cherpak, I. P. Babiichuk, and M. B. Kosmyna, Tech. Phys. Lett. **28**, 221 (2002).
[7] S. G. Lim, S. Kriventsov, T. N. Jackson, J. H. Haeni, D. G. Schlom, A. M. Balbashov, R. Uecker, P. Reiche, J. L. Freeouf, and G. Lucovsky, J. Appl. Phys. **91**, 4500 (2002).
[8] L. F. Edge, D. G. Schlom, S. A. Chambers, E. Cicerrella, J. L. Freeouf, B. Hollander, and J. Schubert, Appl. Phys. Lett. **84**, 726 (2004).
[9] Y. Y. Mi, Z. Yu, S. J. Wang, P. C. Lim, Y. L. Foo, A. C. H. Huan, and C. K. Ong, Appl. Phys. Lett. **90**, 181925 (2007).
[10] D. O. Klenov, D. G. Schlom, H. Li, and S. Stemmer, Jpn. J. Appl. Phys., Part 2 **44**, L617 (2005).
[11] C. J. Forst, K. Schwarz, and P. E. Blochl, Phys. Rev. Lett. **95**, 137602 (2005).
[12] A. A. Knizhnik, I. M. Iskandarova, A. A. Bagatur'yants, B. V. Potapkin, L. R. C. Fonseca, and A. Korkin, Phys. Rev. B **72**, 235329 (2005).
[13] Y. F. Dong, Y. Y. Mi, Y. P. Feng, A. C. H. Huan, and S. J. Wang, Appl. Phys. Lett. **89**, 122115 (2006).
[14] P. W. Peacock and J. Robertson, J. Appl. Phys. **92**, 4712 (2002).
[15] K. Xiong, J. Robertson, and S. J. Clark, Appl. Phys. Lett. **89**, 022907 (2006).
[16] J. L. Tang, J. Zhu, W. F. Qin, J. Xiong, Y. Zhang, and Y. R. Li, Phys. Lett. A **365**, 149 (2007).
[17] S. A. Shevlin, A. Curioni, and W. Andreoni, Phys. Rev. Lett. **94**, 146401 (2005).
[18] P. Delugas, V. Fiorentini, and A. Filippetti, Phys. Rev. B **71**, 134302 (2005).
[19] M. Losurdo, M. M. Giangregorio, M. Luchena, P. Capezzuto, G. Bruno, R.

G. Toro, G. Malandrino, I. L. Fragala, and R. Lo Nigro, Appl. Surf. Sci. **253**, 322 (2006).

[20] E. Cicerrella, J. L. Freeouf, L. F. Edge, D. G. Schlom, T. Heeg, J. Schubert, and S. A. Chambers, J. Vac. Sci. Technol. A **23**, 1676 (2005).

[21] P. Blaha, K. Schwarz, G. Madsen, D. Kvasnicka, and J. Luitz, *WIEN2k, An Augmented Plane Wave Plus Local Orbitals Program for Calculating Crystal Properties* (Vienna University of Technology, Vienna, 2001).

[22] J. P. Perdew, K. Burke, and H. Ernzerhofer, Phys. Rev. Lett. **77**, 3865 (1996).

[23] S. A. Hayward, F. D. Morrison, S. A. T. Redfern, E. K. H. Salje, J. F. Scott, K. S. Knight, S. Tarantino, A. M. Glazer, V. Shuvaeva, P. Daniel, M. Zhang, and M. A. Carpenter, Phys. Rev. B **72**, 054110 (2005).

[24] C. J. Howard, B. J. Kennedy, and B. C. Chakoumakos, J. Phys.: Condens. Matter **12**, 349 (2000).

[25] M. El Kazzi, C. Merckling, G. Delhaye, L. Arzel, G. Grenet, E. Bergignat, and G. Hollinger, Mater. Sci. Semicond. Process. **9**, 954 (2006).

[26] G. Lucovsky, J. L. Whitten, and Y. Zhang, Solid-State Electron. **46**, 1687 (2002).

[27] L. F. Edge, D. G. Schlom, P. Sivasubramani, R. M. Wallace, B. Hollander, and J. Schubert, Appl. Phys. Lett. **88**, 112907 (2006).

[28] Y. C. Yeo, J. Appl. Phys. **92**, 7266 (2002).

[29] R. F. Egerton, *Electron Energy-Loss Spectroscopy in the Electron Microscope* (Springer, New York, 1996).

[30] R. Saniz, L. H. Ye, T. Shishidou, and A. J. Freeman, Phys. Rev. B **74**, 014209 (2006).

[31] A. Moewes, S. Stadler, R. P. Winarski, D. L. Ederer, M. M. Grush, and T. A. Callcott, Phys. Rev. B **58**, R15951 (1998).